MULTI-GRID METHOD FOR PERIODIC HETEROGENEOUS MEDIA. PART 2: MULTISCALE MODELING
AND QUALITY CONTROL IN MULTIDIMENSIONAL CASE

Jacob Fish and Vladimir Belsky
Department of Civil Engineering and Scientific Computation
Research Center,
Rensselaer Polytechnic Institute, Troy, NY 12180

ABSTRACT

A multi-grid method for a periodic heterogeneous medium in multidimensions is developed. Based on the homogenization theory special intergrid transfer operators have been developed to simulate a low frequency response of the boundary value problem with oscillatory coefficients. An adaptive strategy is developed to form a nearly optimal two-scale computational model consisting of the finite element mesh entirely constructed on the microscale in the regions identified by the idealization error indicators, while elsewhere, the modeling level is only sufficient to capture the response of homogenized medium. Numerical experiments show the usefulness of the proposed adaptive multi-level procedure for predicting a detailed response of composite specimens.

1. Introduction

The computational complexity of modeling large scale composite structures is enormous primarily due to the multiple scales involved. For example, the typical size of the structure (an airplane or a car) is of the order of magnitude of tens of meters, while the diameter of the fastener hole is of the order of millimeters. Prediction of micromechanical failure modes necessitates considerations at even smaller scales. The useful life of a structure depends on the quality of modeling at each scale and the ability of a reliable transfer of the appropriate information between various modeling levels. Thus, the need for reliable analysis techniques at several different scales is crucial.

Mathematical homogenization theory [1-3] or its engineering counterpart [4] have been traditionally used as a primary tool for analyzing heterogeneous medium. Based on the assumptions of microstructure periodicity and uniformity of macroscopic fields within a unit cell domain, homogenization theory decomposes the boundary value problem in a heterogeneous medium into the unit cell (micro) problem and the global (macro) problem. The computational sequence consists of three steps: (i) solution of the unit cell problem and evaluation of the homogenized material properties, (ii) solution of the

macro-problem and (iii) post-processing on the micro-level. Reliability of computations in a heterogeneous medium is strongly linked to the validity of the two basic assumptions (periodicity and uniformity), introduced by the classical homogenization theory. The issue of statistical periodicity has been investigated in [5] and is not addressed here. Instead, we concentrate on the issue of uniformity of macroscopic fields (or absence of it) within the unit cell domain. These studies are motivated by the well known fact that in the high gradient regions the macroscopic fields are rapidly varying and their uniformity within the unit cell domain is highly questionable.

This paper proposes an alternative to the classical homogenization that abandons the classical hypothesis of uniformity of the macroscopic fields within the unit cell domain. By this approach solution obtained from the mathematical homogenization theory is only used to simulate the global response of the discrete heterogeneous medium. The proposed computational scheme can be viewed as a generalization of the multi-grid method for the periodic heterogeneous medium. Within this framework the mathematical homogenization theory serves as a mechanism for capturing the lower frequency response of the discrete heterogeneous medium, while the classical relaxation techniques are employed to capture the oscillatory response.

Previous studies[6] have indicated that for problems in heterogeneous medium eigenvalues corresponding to the lower frequencies are not smooth and thus the classical bi- or tri- linear operators are not suitable for data transfer between the grids. For 1-D problems it has been found [6] that the rate of convergence is governed by the factor $q/(4-q)$, where $0 < q \leq 1$ depends on the microstructure. This estimate reveals that the rate of convergence increases with the increase in material heterogeneity.

The paper focuses on the issues of adaptive multiscale modeling and fast iterative solution algorithms for problems in heterogeneous media. We will attempt to construct a nearly optimal two-scale computational model consisting of the finite element mesh entirely constructed on the microscale in the regions where there is a necessity to do so, while elsewhere, the modeling level will be only sufficient to capture the response of homogenized medium. The microscale reduction error indicators described in section 5, are used to assess the quality of homogenized model, and to identify the regions where the homogenized model should be replaced by a model reflecting the details of the microstructure.

Once the two-scale model is constructed, the multigrid-like solvers in the form of MLAT [7] and/or FAC [8,9] are employed due to their linear asymptotic rate of convergence, as opposed to the roughly quadratic growth in CPU time versus the problem size in the case of the direct coupled global-local solutions (or, to be more precise,

NB^2 ,where N and B are the problem size and the bandwidth, respectively). We show that it is possible to obtain even faster convergence for the case of differential equations with highly oscillatory periodic coefficients if special intergrid transfer operators developed in section 3 are utilized.

The outline of this paper is as follows. Problem statement and objectives are formulated in section 2. Special purpose intergrid transfer operators for a periodic heterogeneous medium are derived in section 3. Section 4 describes an adaptive two-scale computational procedure for periodic heterogeneous medium. Microscale reduction error indicators and estimators aimed at quantifying the quality of homogenization and steering the adaptive process are given in section 5. Numerical experiments conclude the manuscript.

2. Problem statement

In modeling heterogeneous media one can adopt two different points of view:

2.1 Mathematical modeling on the microscale

In this scenario each phase (fiber and matrix) is assumed to possess homogeneous properties and obey equilibrium and kinematical equations as well as compatibility and traction continuity conditions between the phases. The corresponding strong form of the boundary value problem for a linear elastostatics is given by

$$
\begin{aligned}
\sigma_{ij,j} &= b_i & on \quad \Omega \\
\sigma_{ij} &= D_{ijkl}\varepsilon_{kl} & on \quad \Omega \\
\varepsilon_{ij} &= u_{(i,j)} & on \quad \Omega \\
u_i &= \bar{u}_i & on \quad \Gamma_u \\
\sigma_{ij}n_j &= t_i & on \quad \Gamma_t \\
[\sigma_{ij}n_j]_{\Gamma_{int}} &= 0 & [u_i]_{\Gamma_{int}} = 0
\end{aligned}
\tag{1}
$$

where σ_{ij} and ε_{ij} are the components of the stress and strain tensors, respectively; b_i and t_i represent the body forces and prescribed boundary tractions on the boundary Γ_t, respectively; u_i are the components of the displacement vector; $\bar{u}_i$ are the prescribed displacements on the boundary Γ_u; D_{ijkl} represent the components of the symmetric

positive definite fourth order constitutive tensor; Ω is a problem domain. The last two equations correspond to traction and displacement continuity conditions on the interface, Γ_{int}, between the microconstituents. $[\ldots]_{\Gamma_{int}}$ denotes the jump operator on Γ_{int}. Symmetric gradient is denoted by $\varphi_{(i,j)} = (\varphi_{i,j} + \varphi_{j,i})/2$. Standard tensorial notation with summation over the repeated indexes is employed.

2.2 Mathematical modeling on the macroscale

Following the classical homogenization theory [1-3] the asymptotic solution of the boundary value problem (1) for the periodic heterogeneous medium can be obtained using two-term double scale asymptotic expansion

$$u_i(x, y) = u_i^0(x) + \varepsilon u_i^1(x, y) \tag{2}$$

where

$$u_i^1(x, y) = h_{ikl}(y)\varepsilon_{kl}^0(x) \qquad \varepsilon_{kl}^0(x) = u_{(k, l)}^0 \tag{3}$$

and x is a macroscopic co-ordinate vector, $y = x/\varepsilon$ is a microscopic position vector. The parameter ε is a representative unit cell size, which is very small in comparison with the dimensions of the problem domain. The periodicity of the microstructure implies that $F(x, y + kY) = F(x, y)$, where vector Y is a basic period of the microscopic co-ordinate system; k is a nonzero integer.

In the representation (3) $h_{ikl}(y)$ is the Y-periodic function, which can be found from the solution of the boundary value problem on the unit cell domain θ subjected to periodic boundary conditions:

$$(D_{ijkl}(h_{(k, l)mn} + \delta_{km}\delta_{ln}))_j = 0 \qquad on \quad \theta \tag{4}$$

where δ_{ij} is a Kronecker delta.

The corresponding expansion of the strain tensor is given

$$\varepsilon_{ij} = (\delta_{ik}\delta_{jl} + h_{(i,j)kl})\varepsilon_{kl}^0 + O(\varepsilon) \tag{5}$$

The macroscopic displacement field $u_i^0(x)$ is the solution of the following boundary value problem with homogenized coefficients

$$(\tilde{D}_{ijkl}u^0_{(k,\,l)})_j = f_i \qquad on \quad \Omega$$

$$u^0_i = \bar{u}_i \qquad on \quad \Gamma_u \tag{6}$$

$$\tilde{D}_{ijkl}u^0_{(k,\,l)}n_j = t_i \qquad on \quad \Gamma_t$$

where

$$\tilde{D}_{mnpq} = \frac{1}{\theta_Y}\int_\theta (\delta_{im}\delta_{jn} + h_{(i,\,j)mn})D_{ijkl}(\delta_{kp}\delta_{lq} + h_{(k,\,l)pq})d\theta \tag{7}$$

and θ_Y is the volume of the unit cell.

Each of the two mathematical models is discretized using a finite element method. The corresponding discrete models are termed as micro and macro finite element meshes, each may have various levels of mesh refinement.

It is the primary goal of the paper to find a numerical solution of the micro finite element model. A direct solution of the system of equations resulting from such a discretization is usually computationally not feasible since it may involve over a million of unknowns. On the other hand, the finite element solution of the macro-model (6)-(7) is generally feasible and can be utilized to capture the lower frequency response of the discrete heterogeneous system, while various smoothing procedures would be very efficient in capturing the oscillatory response of a heterogeneous medium. This suggests that a multi-grid like approach is a natural choice for solving discrete systems constructed on the microscale.

3. The intergrid transfer operators for a periodic heterogeneous medium in multidimensions

In this section we focus on the central issue of constructing the intergrid transfer operators for a periodic heterogeneous medium in multidimensions. The structure of the intergrid transfer operators between the discrete heterogeneous and corresponding homogenized media is defined on the basis of the discrete form of the double scale asymptotic expansion:

$$u_i = (N_{ia}(x) + \varepsilon h_{ijk}(y)N_{(j,\,k)a}(x))d_a \tag{8}$$

where $N_{ia}(x)$ and $N_{(j,\,k)a}(x)$ are the displacement and strain interpolants in the

macro-mesh, denoted by

$$u_i^0 = N_{ia}d_a \qquad and \qquad \varepsilon_{ij}^0 = N_{(i,j)a}d_a \qquad (9)$$

and d_a are the corresponding nodal displacements. Hereinafter, capital subscripts $A, B, C, \ldots$ are reserved for the fine grid (micro mesh) degrees-of-freedom, while lower-case subscripts $a, b, c, \ldots$ denote auxiliary coarse grid (macro mesh) degrees-of-freedom.

Since the product εh_{ijk} in equation (4) is independent of the choice of ε, it is more convenient to analyze the unit cell problem in the co-ordinates of the physical domain; i.e., $\varepsilon h_{ijk}(y) = h_{ijk}(x) = O(\varepsilon)$. Thus substituting the discrete form of the unit cell solution, $h_{ijk} = N_{iB}(x)d_{jkB}$, into equation (8) yields

$$u_i = (N_{ia} + N_{iB}N_{(j,k)a}d_{jkB})d_a \qquad (10)$$

With this introduction the problem of the coarse grid correction is now stated in the following proposition.

Proposition

Let the coarse grid correction problem be formulated on the basis of the interpolation defined in equation (10) and let

$$A_{ab}d_b = r_a \qquad (11)$$

be the coarse grid correction problem, where A_{ab} is the stiffness matrix of the boundary value problem (6) with homogenized material properties (7) in the auxiliary macro-mesh, and r_a is the respective restriction of the micro-mesh residual vector.

Then in the limit as $\varepsilon \to 0$ the stiffness matrix A_{ab} coincides with the restriction of the stiffness matrix of the boundary value problem on the micro-mesh (1).

Proof:

Let Q_{Aa} be a standard (for the second order differential equations) bi-linear or tri-linear coarse-to-fine grid prolongation operator. The nodal degrees of freedom in the two meshes are then related by

$$d_A = Q_{Aa}d_a \tag{12}$$

The hypothesis of $\varepsilon \to 0$ is equivalent to the infinitesimally small mesh size in the micro-mesh, and thus, without loss of generality, the shape functions on the auxiliary grid can be represented as a linear combination of the shape functions on the micro-mesh, i.e.

$$N_{ia}(x) = N_{iA}(x)Q_{Aa} \tag{13}$$

where the coefficients of linear expansion Q_{Aa} follow from the relation $N_{ia}d_a = N_{iA}d_A = N_{iA}Q_{Aa}d_a$.
Inserting (13) into (10) yields

$$u_i(x) = N_{iA}(Q_{Aa} + N_{(j,k)a}d_{jkA})d_a \tag{14}$$

To construct the homogenization-based prolongation operator $\tilde{Q}_{Aa}$ we evaluate u_i at the micro mesh nodes $x_{\underline{B}}$

$$u_i(x_{\underline{B}}) = d_B = N_{iA}(x_{\underline{B}})(Q_{Aa} + N_{(j,k)a}(x_{\underline{B}})d_{jkA})d_a \tag{15}$$

where underlined subscripts indicate no summation over the repeated indices. Note that the displacement along the spatial co-ordinate i at the node $x_{\underline{B}}$ corresponds to the degree-of-freedom B in the micro grid, i.e. $u_i(x_{\underline{B}}) \equiv d_B$ and $N_{iA}(x_{\underline{B}}) \equiv \delta_{AB}$. Thus

$$d_B = \tilde{Q}_{Ba}d_a \tag{16}$$

where the homogenization-based prolongation operator is defined as follows

$$\tilde{Q}_{Ba} = Q_{Ba} + N_{(j,k)a}(x_{\underline{B}})d_{jkB} \tag{17}$$

It remains to show that $\tilde{Q}_{Aa}$ restricts the stiffness matrix of the micro-mesh, A_{AB}, to the coarse grid in such a way that the resulting stiffness matrix $A_{ab} = \tilde{Q}^*_{aA}A_{AB}\tilde{Q}_{Bb}$ coincides with the stiffness matrix of the macro problem (6) with homogenized material properties (7) in the limit as $\varepsilon \to 0$.

For this purpose we evaluate the strain field by taking the symmetric gradient of the displacement field given in (8):

$$\varepsilon_{ij} = (N_{(i,j)a}(x) + h_{(i,j)kl}(x)N_{(k,l)a}(x))d_a + O(\varepsilon) \tag{18}$$

In the limit as $\varepsilon \to 0$ the last term can be neglected resulting in the following strain approximation

$$
\begin{aligned}
\varepsilon_{ij} &= (\delta_{ik}\delta_{jl} + h_{(i,j)kl})N_{(k,l)a}d_a \\
&= N_{(i,j)A}(Q_{Aa} + N_{(k,l)a}d_{klA})d_a
\end{aligned}
\tag{19}
$$

Note that an identical strain approximation can be obtained by direct discretization of the two-term asymptotic strain expansion given in (5).

The macro-mesh stiffness matrix is given by:

$$
A_{ab} = \int_{\Omega} N_{(i,j)a}\tilde{D}_{ijkl}N_{(k,l)b}d\Omega
\tag{20}
$$

$$
= \sum_{cells}\frac{1}{\theta_Y}\int_{\theta} N_{(m,n)a}N_{(p,q)b}d\theta \int_{\theta}(\delta_{im}\delta_{jn} + h_{(i,j)mn})D_{ijkl}(\delta_{kp}\delta_{lq} + h_{(k,l)pq})d\theta
$$

Further exploiting the hypothesis of the infinitesimality of the unit cell, as $\varepsilon \to 0$, we note that

$$
N_{(i,j)a}(x_{\underline{B}}) = N^I_{(i,j)a} = const \qquad \forall x_{\underline{B}} \in \theta^I
\tag{21}
$$

where the superscript I denotes the unit cell number.

Finally, inserting (21) into (20) yields:

$$
A_{ab} = \int_{\Omega} \tilde{Q}_{Aa}N_{(i,j)A}D_{ijkl}N_{(k,l)B}\tilde{Q}_{Bb}d\Omega = \tilde{Q}^*_{aA}A_{AB}\tilde{Q}_{Bb}
\tag{22}
$$

which completes the proof of the proposition.

So far the homogenization-based intergrid transfer operators $(\tilde{Q}, \tilde{Q}^*)$ have been derived assuming that $\varepsilon \to 0$. In practice the value of ε is finite, requiring reformulation of the intergrid transfer operators to maintain C^o continuity of the prolongated displacement field in the micro mesh. It should be noted that a direct application of the prolongation operator (17) does not uniquely determines the displacement field on the boundaries of the unit cells, since the macroscopic strain field $N_{(j,k)a}(x_{\underline{B}})d_a$ is a C^{-1} continuous function, i.e., it is discontinuous on the boundaries of the macro-elements. Consequently, the prolongated solution is also discontinuous at the interface

between the unit cells, overlapping different macro-elements.

To develop a homogenization-based prolongation operator $\tilde{Q}$, that generates C^o continuous displacements, it is necessary to construct a C^o continuous strain field in a macro-mesh ε^*_{kl} defined as

$$\varepsilon^*_{kl} = N_a \varepsilon_{kl}(x_a) \tag{23}$$

where $\varepsilon_{kl}(x_a)$ are nodal strain values in the macro-mesh and N_a are the corresponding strain field shape functions. Nodal strain values are typically found by weakly enforcing the equality between the discontinuous finite element strains and their continuous counterpart [10]. By this technique the projection operator C_{ag} is formed to project strain values from a set of sampling points to finite element nodes in the macro-mesh:

$$\varepsilon_{kl}(x_a) = C_{ag} \varepsilon_{kl}(x_g) = C_{ag} N_{(k, l)b}(x_g) d_b \tag{24}$$

where the sampling points, x_g, can be either Gauss points, reduced Gauss points or finite element nodes [10].

Substituting (23) and (24) into (17) and evaluating the displacement field at the finite element nodes in the micro-mesh yields the following expression for the *continuous homogenization-based* prolongation operator:

$$\tilde{Q}_{Aa} = Q_{Ab}(\delta_{ab} + C_{bg} N_{(k, l)a}(x_g) d_{kl\underline{A}}) \tag{25}$$

In the numerical examples considered in this paper projection operator C_{ag} was constructed on the patch-by-patch basis as described in [10]. In the case of a 4-node rectangular element it amounts to computing the nodal strain values by averaging the corresponding strain values evaluated at the element centroids, connected to the node.

Remark: In practice one has to deal with several different types of unit cells such as in the case of laminated composites where each layer is composed of different unit cells. Even though the macro strain field has been projected to be C^o continuous, the prolongated displacement field might still be incompatible at the interface between dissimilar unit cells. This requires further modification of the continuous homogenization-based prolongation operator at the interface between the unit cells of different types.

This is accomplihed by introducing a transition layer of unit cells at the interface between dissimilar unit cells. The formulation of the unit cell problem in the transition region differs from the interior unit cell in the way the boundary conditions are prescribed.

To clarify this point we consider a transition layer, B^*, in a laminated composite at the interface between two dissimilar layers A and B as shown in Fig. 1. The microstructure in the transition region, B^*, is identical to that in the layer B. The boundary conditions applied to the unit cell in the transition region are of the following categories:

(i) On the faces (edges in 2-D) orthogonal to the interface, the boundary conditions are periodic, i.e., displacements d_{ijA} are equal on the opposite sides of the unit cell.

(ii) On the faces parallel to the interface, the non-homogeneous Dirichlet boundary conditions are assumed instead. The prescribed displacement values are assumed to be equal to those in the neighboring layer. In general, the value of these displacements is not equal to those on the opposite sides of the unit cell.

The unit cell boundary value problems are solved in the following sequence (3-D case). First solve for the interior unit cells (with all periodic boundary conditions). This is followed by the unit cells at the interface between two dissimilar layers (with partially periodic and Dirichlet boundary conditions). Then the unit cells along the edge connecting four different layers (with partially periodic and Dirichlet boundary conditions), and finally the unit cells connected to eight different unit cells (with Dirichlet boundary conditions only).

4. Multiscale solution algorithm for heterogeneous media

In this section we present the formulation of multiscale solution algorithm for problems in a periodic heterogeneous medium where one or more regions are modeled on the microscale, while elsewhere the medium is treated as homogenized. Our formulation is applicable to general three-dimensional domains with unlimited number of local regions, although for simplicity, illustrations are limited to two-dimensional problems with a single local region. Attention is restricted to a two-level scheme.

4.1 Problem definition and notation

Consider a heterogeneous medium on $\tilde{\Omega}$ which is formed by a special periodicity of a unit cell. Suppose, that the Microscale Reduction Error (MRE) indicator to be described in section 5, indicates, that the classical homogenization procedure is not valid on the portion of the problem domain, denoted by $\Omega \subset \tilde{\Omega}$. Therefore, the optimal computational model consists of the finite element grid $\hat{G}$ on $\hat{\Omega} = \tilde{\Omega}/\Omega$, where the elements are assumed to possess homogenized material properties, and a finite element grid G, with much smaller elements constructed on the microscale.

The micro-grid G, is partitioned as follows:

$$G = G_I \cup G_L \tag{26}$$

10

where G_I are the micro-grid nodes at the interface Γ_I between the two regions, and G_L are the interior micro-grid nodes as shown in Fig. 2.

Likewise the macro-grid $\hat{G}$ is partitioned in a similar fashion:

$$\hat{G} = \hat{G}_I \cup \hat{G}_G \tag{27}$$

where $\hat{G}_I$ are the macro-grid nodes at the interface Γ_I, which do not have to coincide with the nodes in G_I, and $\hat{G}_G$ are the remaining macro-grid points.

We further define an auxiliary grid $\tilde{G}$ on $\tilde{\Omega}$, where the entire finite element mesh is modeled with homogenized material properties. The grid $\tilde{G}$ is aimed at capturing the lower frequency response of the two-scale grid model $G \cup \hat{G}$. The auxiliary grid is partitioned as follows:

$$\tilde{G} = \tilde{G}_I \cup \tilde{G}_L \cup \tilde{G}_G \tag{28}$$

where $\tilde{G}_I = \hat{G}_I, \tilde{G}_G = \hat{G}_G$; the grid $\tilde{G}_L$ represents auxiliary grid points on Ω as shown in Fig. 2.

For information transfer between the micro- and macro- grids we employ continuous homogenization-based prolongation operator $\tilde{Q}$ derived in section 3, which is partitioned into two blocks for convenience. The first denoted by $\hat{Q}$, relates nodal displacements in the macro grid $\hat{G}$ to those in the micro grids G at the interface Γ_I only:

$$\hat{Q}:\hat{G} \rightarrow G_I \tag{29}$$

where

$$\hat{Q} = \begin{bmatrix} \tilde{Q}_{II} & \tilde{Q}_{IG} \end{bmatrix} \tag{30}$$

such that

$$\tilde{Q}_{II}:\tilde{G}_I \rightarrow G_I \qquad and \qquad \tilde{Q}_{IG}:\tilde{G}_G \rightarrow G_I \tag{31}$$

Note, that as opposed to the standard linear prolongation operator, which relates the information at the interface only, continuous homogenization-based operator $\tilde{Q}_{IG}$ is a function of $\nabla_s N(x_g)$ on $\tilde{\Omega}$ resulting in the information flow from the interior to the boundary and vice versa.

Likewise, we define the second block of the continuous homogenization-based prolon-

gation operator denoted by $\bar{Q}$ which relates the information between the auxiliary coarse grid and the interior micro grid nodes:

$$\bar{Q}:\tilde{G} \to G_L \tag{32}$$

which is partitioned as

$$\bar{Q} = \begin{bmatrix} \tilde{Q}_{LI} & \tilde{Q}_{LL} \end{bmatrix} \tag{33}$$

such that

$$\tilde{Q}_{LI}:\tilde{G}_I \to G_L \qquad and \qquad \tilde{Q}_{LL}:\tilde{G}_L \to G_L \tag{34}$$

Consequently, the continuous homogenization-based prolongation operator $\tilde{Q}$ can be structured as follows:

$$\tilde{Q} = \begin{bmatrix} \tilde{Q}_{II} & 0 & \tilde{Q}_{IG} \\ \tilde{Q}_{LI} & \tilde{Q}_{LL} & 0 \end{bmatrix} \tag{35}$$

The continuous homogenization-based restriction operators $\tilde{Q}^*:G \to \tilde{G}$ and $\hat{Q}^*:G_I \to \hat{G}$ are conjugated to $\tilde{Q}$ and $\hat{Q}$, and are schematically denoted as

$$\tilde{Q}^* = \begin{bmatrix} \tilde{Q}_{II}^* & \tilde{Q}_{LI}^* \\ 0 & \tilde{Q}_{LL}^* \\ \tilde{Q}_{IG}^* & 0 \end{bmatrix} \qquad and \qquad \hat{Q}^* = \begin{bmatrix} \tilde{Q}_{II}^* \\ \tilde{Q}_{IG}^* \end{bmatrix} \tag{36}$$

For subsequent derivations we will introduce the following notation:

$\tilde{u} = \begin{bmatrix} \tilde{u}_I & ;\tilde{u}_L & ;\tilde{u}_G \end{bmatrix}^*$ — auxiliary grid displacement vector, where $\tilde{u}_I \in \tilde{G}_I$, $\tilde{u}_L \in \tilde{G}_L$, $\tilde{u}_G \in G_G$.

$\hat{u} = \begin{bmatrix} \tilde{u}_I & ;\tilde{u}_G \end{bmatrix}^*$ — macro-grid displacement vector on $\hat{G}$.

$u = \begin{bmatrix} u_I & ;u_L \end{bmatrix}^*$ — micro-grid displacement vector, such that $u_I \in G_I$ and $u_L \in G_L$;

12

$$\tilde{A} = \begin{bmatrix} \tilde{A}_{II} & \tilde{A}_{IL} & \tilde{A}_{IG} \\ \tilde{A}_{LI} & \tilde{A}_{LL} & 0 \\ \tilde{A}_{GI} & 0 & \tilde{A}_{GG} \end{bmatrix}$$ - auxiliary grid stiffness matrix on $\tilde{G}$;

$$\hat{A} = \begin{bmatrix} \hat{A}_{II} & \hat{A}_{IG} \\ \hat{A}_{GI} & \hat{A}_{GG} \end{bmatrix}$$ - macro-grid stiffness matrix on $\hat{G}$, such that $\hat{A}_{GG} = \tilde{A}_{GG}$ and $\hat{A}_{IG} = \tilde{A}_{IG}$;

$$A = \begin{bmatrix} A_{II} & A_{IL} \\ A_{LI} & A_{LL} \end{bmatrix}$$ - micro-grid stiffness matrix on G;

$$\tilde{f} = \begin{bmatrix} \tilde{f}_I \vdots \tilde{f}_L \vdots \tilde{f}_G \end{bmatrix}^*$$ - auxiliary grid force vector, where $\tilde{f}_I, \tilde{f}_L, \tilde{f}_G$ are nodal forces acting on grids $\tilde{G}_I, \tilde{G}_L, \tilde{G}_G$, respectively.

$$\hat{f} = \begin{bmatrix} \hat{f}_I \vdots \hat{f}_G \end{bmatrix}^*$$ - macro-grid force vector acting on $\hat{G}$, such that $\hat{f}_G = \tilde{f}_G$;

$$f = \begin{bmatrix} f_I \vdots f_L \end{bmatrix}^*$$ - micro-grid force vector, where f_I and f_L are nodal forces acting on grids G_I and G_L, respectively.

We note that the displacement vectors $\tilde{u}$ and $\hat{u}$ are related via orthogonal assembly operator L given by

$$L = \begin{bmatrix} I & 0 & 0 \\ 0 & 0 & I \end{bmatrix} \tag{37}$$

where I is an identity matrix of an appropriate size, such that

$$\hat{u} = L\tilde{u} \tag{38}$$

We are now in a position to formulate an algebraic system of equations for the two-

scale linear elasticity problem in heterogeneous media. It consists of finding a pair of nodal displacement vectors $(\hat{u}, u)$ such that

$$1/2((\hat{A}\hat{u}, \hat{u}) + (Au, u)) - (\hat{f}, \hat{u}) - (f, u) \Rightarrow \min_{(\hat{u}, u)} \quad (39)$$

subjected to the compatibility condition at the interface

$$u_I = \hat{Q}\hat{u} \quad (40)$$

Minimization of (39) with respect to $(\hat{u}, u)$ subjected to the interface condition (40) yields a system of linear equations:

$$\begin{bmatrix} (\hat{A} + \hat{Q}^* A_{II} \hat{Q}) & \hat{Q}^* A_{IL} \\ A_{LI}\hat{Q} & A_{LL} \end{bmatrix} \begin{bmatrix} \hat{u} \\ u_L \end{bmatrix} = \begin{bmatrix} \hat{f} + \hat{Q}^* f_I \\ f_L \end{bmatrix} \quad (41)$$

The system of linear equations (41) can be solved either directly or iteratively. The direct solver is not well suited for an adaptive computational environment, where the region requiring a more detailed interrogation, is not known a priori.

It is our objective to develop an iterative solution procedure, which exploits the solution of the auxiliary problem on $\tilde{G}$ in order: (i) to identify the regions where the homogenized finite element model is inadequate, and (ii) to predict the lower frequency response of the two-scale model.

Section 5 deals with the first item, while in section 4.2 we focus on developing a two-scale iterative solution scheme.

4.2. Iterative two-scale solution procedures

The three-step iterative solution procedure based on minimization of energy functional (39) on various subspaces is given below:

Step 1.

Find the correction $\tilde{v}^i$ which minimizes the two-scale energy functional (39) on the subspace of the auxiliary grid functions, i.e.,

$$1/2((\hat{A}(\hat{u}^i + L\tilde{v}^i), \hat{u}^i + L\tilde{v}^i) + (A(u^i + \tilde{Q}\tilde{v}^i), u^i + \tilde{Q}\tilde{v}^i))$$

$$- (\hat{f}, \hat{u}^i + L\tilde{v}^i) - (f, u^i + \tilde{Q}\tilde{v}^i) \Rightarrow \min_{\tilde{v}^i} \tag{42}$$

where the superscripts refer to the iteration count.

Note that the auxiliary grid correction $\tilde{v}^i$ has a similar partitioning to $\tilde{u}$, i.e. $\tilde{v} = \begin{bmatrix} \tilde{v}_I & ; \tilde{v}_L & ; \tilde{v}_G \end{bmatrix}^*$ and $\hat{v} = \begin{bmatrix} \tilde{v}_I & ; \tilde{v}_G \end{bmatrix}^*$.

A direct minimization of (42) with respect to $\tilde{v}^i$ yields:

$$(L^*\hat{A}L + \tilde{Q}^*A\tilde{Q})\tilde{v}^i = L^*(\hat{f} - \hat{A}\hat{u}^i) + \tilde{Q}^*(f - Au^i) \tag{43}$$

The first term on the left hand side represents the assembled form of the macro-grid stiffness matrix. In section 3 we have shown that for an infinitesimally small unit cell the second term represents an assembled form of the stiffness matrix on the auxiliary grid G_L, i.e.:

$$\lim_{\varepsilon \to 0} (L^*\hat{A}L + \tilde{Q}^*A\tilde{Q}) = \tilde{A} \tag{44}$$

In practice, however, the value of the representative unit cell size ε is finite, and thus (44) is satisfied only approximately. Nevertheless, for the purpose of approximating the auxiliary grid correction $\tilde{v}^i$ we will replace the Jacobian matrix in (43) by $\tilde{A}$. In the adaptive environment this approximation will significantly reduce computational cost, since only a single factorization of the auxiliary stiffness matrix is required, independent of the refinement process.

<u>Step 2.</u>

Once the auxiliary grid correction has been carried out it is necessary to update the solution in the auxiliary grid:

$$\tilde{u}^{i+1} = \tilde{u}^i + \omega\tilde{v}^i \qquad \hat{u}^{i+1} = \hat{u}^i + \omega L\tilde{v}^i \qquad u^{i+1} = u^i + \omega\tilde{Q}\tilde{v}^i \tag{45}$$

The relaxation parameter is introduced to account for the approximation introduced in (44) as a result of a finite size of the unit cell. The relaxation parameter is found from a 1-D minimization of the energy functional along the direction $\tilde{v}^i$ evaluated in the previous step (43):

$$1/2((\hat{A}(\hat{u}^i + \omega L\tilde{v}^i), \hat{u}^i + \omega L\tilde{v}^i) + (A(u^i + \omega\tilde{Q}\tilde{v}^i), u^i + \omega\tilde{Q}\tilde{v}^i))$$

$$- (\hat{f}, \hat{u}^i + \omega L\tilde{v}^i) - (f, u^i + \omega\tilde{Q}\tilde{v}^i) \Rightarrow \min_{\omega} \tag{46}$$

which yields

$$\omega = \frac{(L^*(\hat{f} - \hat{A}\hat{u}^i) + \tilde{Q}^*(f - Au^i), \tilde{v}^i)}{((L^*\hat{A}L + \tilde{Q}^*A\tilde{Q})\tilde{v}^i, \tilde{v}^i)} \tag{47}$$

<u>Step 3.</u>
Find the correction v_L^i on the micro-grid, which minimizes the energy functional on the subspace of the functions on the micro-grid G_L, i.e. keeping $\hat{u}^i$ fixed:

$$1/2((\hat{A}\hat{u}^i, \hat{u}^i) + (A(u^i + v^i), u^i + v^i)) - (\hat{f}, \hat{u}^i) - (f, u^i + v^i) \Rightarrow \min_{v^i} \tag{48}$$

where $v_I^i = 0$ on Γ_I to maintain compatibility.
The direct minimization of (48) yields

$$A_{LL}v_L^i = f_L - A_{LI}\hat{Q}\hat{u}^i - A_{LL}u_L^i \tag{49}$$

If (49) is directly solved and

$$u_L^{i+1} = u_L^i + v_L^i \tag{50}$$

then the three-steps iterative process described is in the spirit of FAC algorithm [8,9], subsequently to be referred as FAC-Comp.

It is important to note that since the unit cell is very small, the number of degrees-of-freedom in micro-grid could be larger than in the macro-grid. Secondly, the solution behavior in the micro-grid is highly oscillatory with a lower frequency response similar to that in the auxiliary mesh. These two observations suggest to replace the direct solution of (49) by smoothing of the form given by

$$u_L^{i+1} = u_L^i + \tau^i P_{LL}(f_L - A_{LI}\hat{Q}\hat{u}^i - A_{LL}u_L^i) \tag{51}$$

where P_{LL} is a preconditioner on the micro-grid G_L and τ^i is a relaxation parameter given by

$$\tau^i = \frac{(f_L - A_{LI}\hat{Q}\hat{u}^i - A_{LL}u_L^i, v_L^i)}{(A_{LL}v_L^i, v_L^i)} \tag{52}$$

where $v_L^i = P_{LL}(f_L - A_{LI}\hat{Q}\hat{u}^i - A_{LL}u_L^i)$.

This variant has similar characteristics to the linear version of MLAT [7], and will be termed as MLAT-Comp.

5. The microscale reduction error estimators and indicators

5.1. Formulation

In this section we quantify idealization errors associated with homogenization of periodic heterogeneous medium and present their use in the adaptive procedure. The proposed Microscale Reduction Error (MRE) estimator is based on assessing the uniform validity of the double scale asymptotic expansion [1-3], which is given by a rapidly decreasing asymptotic sequence:

$$u_i^\varepsilon = u_i^0(x) + \varepsilon H_{ijk}(y)u_{(j,k)}^0(x) + \varepsilon^2 P_{ijkl}(y)u_{j,kl}^0(x) + O(\varepsilon^3) \tag{53}$$

Following [1-3] the Y-periodic function P_{ijkl} is found from the higher order equilibrium equation:

$$\frac{\partial}{\partial y_p}(D_{ipkl}(P_{(k,l)mnj} + H_{kmn}\delta_{lj})) + D_{ijkl}(H_{(k,l)mn} + \delta_{km}\delta_{ln}) - \tilde{D}_{ijmn} = 0 \tag{54}$$

$$on \quad unit \quad cell \quad \theta_Y$$

Problem (54) is solved using finite element method. The resulting asymptotic expansion of the stress field is given by

$$\sigma_{ij} = A_{ijkl}^0(y)u_{(k,l)}^0(x) + \varepsilon A_{ijklq}^1(y)u_{k,lq}^0(x) + O(\varepsilon^2) \tag{55}$$

where

$$A^0_{ijmn}(y) = D_{ijkl}(H_{(k, l)mn} + \delta_{k, m}\delta_{ln})$$

$$A^1_{ijmnp}(y) = D_{ijkl}(P_{(k, l)mnp} + H_{kmn}\delta_{lp})$$

(56)

In the classical homogenization theory only the first term in (55) is considered, while the second term is neglected. Thus, the quality of the homogenization is assessed on the basis of the relative magnitude of the first term neglected to those taken into account. The resulting Microscale Reduction Error estimator is defined as

$$\eta = \frac{\left\| \varepsilon A^1 \nabla^2 u^0 \right\|_{0, \Omega}}{\left\| A^0 \nabla u^0 \right\|_{0, \Omega}}$$

(57)

where $\| \bullet \|_{0, \Omega}$ is a L_2 - norm defined as

$$\|h(x, y)\|_{0, \Omega} = \frac{1}{Y_A}\left(\sum_{i, j} \int_\Omega \int_Y h^2_{ij}(x, y)dYd\Omega \right)^{1/2}$$

(58)

To steer process of adaptivity we define the MRE indicator, which reflects the relative contribution of individual element in the auxiliary mesh to the total microscale reduction error:

$$\eta^e = \beta^e \frac{\left\| \varepsilon A^1_{klq} u^0_{k, lq} \right\|_{0, \Omega^e}}{\left\| A^0_{kl} u^0_{(k, l)} \right\|_{0, \Omega}} \qquad \beta^e = \frac{\Omega}{\Omega^e}$$

(59)

This approach is equivalent to the one employed for discretization error indicator in [11].

3.2. Explicit form of η and η^e in 1D

In this subsection, we derive a close form MRE indicators and estimators for a 1D model problem in order to study various factors affecting the microscale reduction errors.

Closed form solution of (4), (54) for H and P yields:

$$A^0 = \tilde{D} = \left(\frac{1}{h}\int_0^h D^{-1} dy\right)^{-1} = const_1 \tag{60}$$

and

$$A^1 = \frac{\tilde{D}}{h}\int_0^h H dy = const_2 \tag{61}$$

where $\tilde{D}$ are the effective material properties and h is the unit cell size. Inserting (60) and (61) into (57) yields the one-dimensional counterpart of the microscale reduction error estimator is given by

$$\eta = \int_0^h \left(\frac{\tilde{D}}{D(y)} - 1\right) dy \frac{\left\|\frac{d^2 u^0}{dx^2}\right\|_{0,\Omega}}{\left\|\frac{du^0}{dx}\right\|_{0,\Omega}} \tag{62}$$

For the unit cell consisting of two phases with compliances $C_1 = 1/D_1$ and $C_2 = 1/D_2$ (the overall compliance $\tilde{C} = C_1 + C_2$, $\tilde{C} = 1/\tilde{D}$), α the volume fraction, the resulting MRE estimator is given by

$$\eta = h\frac{|C_1 - C_2|}{\tilde{C}}\frac{\alpha(1-\alpha)}{2}\frac{\left\|\frac{d^2 u^0}{dx^2}\right\|_{0,\Omega}}{\left\|\frac{du^0}{dx}\right\|_{0,\Omega}} \tag{63}$$

From the above expression we can identify four factors affecting the microscale reduction error:

1. The size of the unit cell, h.
2. The normalized difference of compliances, $\dfrac{|C_1 - C_2|}{\tilde{C}}$.
3. The fiber volume ratio, $\dfrac{\alpha(1-\alpha)}{2}$.
4. The macro strain gradients, $\left\|\dfrac{d^2 u^0}{dx^2}\right\|_{0,\Omega}$.

It can be seen that the error estimator is asymptotically exact in the sense that the microscale reduction errors vanish if either the normalized strain gradients are negligible, the unit cell is infinitesimally small, the compliances of the microconstituents are almost identical or the volume ratio is close to either zero or one, which corresponds to a homogeneous material.

6. Numerical results

Our numerical experimentation agenda includes two test problems. The first example deals with a square plate containing a centered crack. Geometry, boundary and symmetry conditions, material properties, loading and unit cell description are shown in Fig. 3. The finest level macro-mechanical grid $\tilde{G}$ with homogenized material properties consists of 64 elements along each co-ordinate where each element coincides with the unique unit cell boundaries.

The distribution of homogenization errors as indicated by MRE indicator is shown in Fig. 4a. The micro-grid, G, is placed on the portion of the problem domain, which encompasses the contour of $\eta^e > 1$ as shown in Fig. 4a. For simplicity the grid G on Ω is selected to be of a rectangular shape. Thus the two-scale model consists of a micro-grid in the region encompassed by 12x20 unit cells in the vicinity of the crack tip, while elsewhere $\tilde{\Omega}/\Omega$, the finite element mesh is constructed on the macro-scale.

The multi-grid process was carried out on three different meshes: two-scale (macro-micro) grid and two auxiliary macro-grids. We used V-cycle with 1 pre- and 1 post-smoothing Gauss-Seidel iterations on the two auxiliary levels and 2 pre- and 2 post-smoothing Jacobi iterations on the finest level. As usual, on the coarsest level we used a direct solver. As a termination criterion we used the following tolerance to bound the ratio of the two-scale grid residual norm versus the norm of the right hand side vector, i.e.,

$$\|r\|_1 / \|f\|_1 \leq eps \qquad where \qquad \|v\|_1 = \sum_{i=1}^{n} |v_i| \qquad v \in R^n \qquad \text{(64)}$$

To obtain convergence with tolerance of $eps = 10^{-3}$ it was necessary to carry out 14 cycles using MLAT-Comp algorithm and 7 cycles with FAC-Comp method.

The resulting energy distribution absorbed in a unit cell in the micro-grid is shown in

Fig. 4c. For comparison purpose also shown are the results obtained on the basis of the postprocessing from the classical homogenization theory [12] and the reference solution where the entire problem domain Ω is modeled on the microscale. It can be seen that the postprocessing procedure from the classical homogenization theory significantly underestimates the energy absorbed in the close vicinity to the crack tip. On the other hand in the radius of 2-3 unit cells away from the crack tip the classical homogenization theory is adequate.

In the second example, we consider a laminated plate $[90_4/0_{16}/90_4]_s$ subjected to uniform axial tension. Geometry, boundary and symmetry conditions and the microstructure cross section for the different layers are shown in Fig. 5. We considered Glass-Epoxy composite material with the following material properties: $E_1 = 72.3$ $\nu_1 = 0.22$ and $E_2 = 2.92$ $\nu_2 = 0.35$. The uniform tension load was applied normal to the xy plane. The finest level of macro-grid $\tilde{G}$ consists of 24 elements along the co-ordinate x (thickness direction) and 192 along y, each element coinciding with the unique unit cell.

The distribution of the homogenization errors and the region selected for micromechanical modeling are shown in Fig. 6a. The micro-grid consists of 14,400 elements placed in the region encompassed by 24x24 unit cells in the vicinity of the free edge. The two-grid model contains approximately 38,000 degrees-of-freedom. The multigrid process was carried out on three different meshes: two-scale (macro-micro) grid and two auxiliary macro-grids. We used V-cycle with 1 pre- and 1 post- smoothing Gauss-Seidel iterations on the auxiliary levels; 3 pre- and 3 post- smoothing Jacobi iterations on the finest level and a direct solver on the coarsest level. 1% error of residual (64) was obtained in 8 cycles of MLAT-Comp algorithm and 8 cycles of FAC-Comp method.

Fig. 6b,c,d compare the shear stress distribution in the micro-grid as obtained using two-scale model, homogenization theory and the reference solution. Results are consistent with our previous observations, i.e., inadequacy of the postprocessing technique from the classical homogenization theory in the "hot spots" as opposed to striking accuracy of the two-scale model.

To study boundary layer effect between two dissimilar layers in the axial tension problem we consider a micro-grid of approximately 15,000 degrees-of-freedom on the entire problem domain. The same solution strategy has been employed. It was necessary to perform 5 multi-grid cycles to achieve convergence with tolerance 0.1%. Fig. 7 and Fig. 8 compare the distribution of peeling stress σ_x and shear stress σ_{xy} as

obtained using the postprocessing from the classical homogenization theory and the finite element solution of the discrete heterogeneous media. It can be seen that except for the close vicinity to the free edge the values of σ_x as obtained with the two methods are in good agreement. On the other hand the distribution of shear stress σ_{xy} differs not only in the vicinity of the free edge, but along the entire interface between the two dissimilar layers. The finite element solution of the discrete heterogeneous model shows oscillatory shear stresses developed along the entire interface, while the solution of homogenized problem shows no such stress concentration. The magnitude of these shear stresses is roughly $1/3$ of the shear stresses developed at the interface, but even so, these interface shear stresses may significantly affect the propagation of delamination cracks emanating from the free edge.

The primary reason why the postprocessing technique fails to detect these interface shear stresses is because it permits displacement incompatibility within a unit cell at the interface between dissimilar layers. On the other hand a finite element solution of the discrete heterogeneous model enforces such compatibility exactly, giving rise to oscillatory shear stresses at the interface.

In the last numerical example we study the effectiveness of MLAT-Comp algorithm for solving very large two-scale models. The problem domain, boundary conditions, loading, and the unit cell model are the same as in the first example. The two-scale model contained a micromechanical finite element mesh in the region of 176x176 unit cells in the vicinity of the crack tip, while elsewhere, the finite elements were treated as homogenized. The macro-mechanical finite element mesh consists of 352 elements along each co-ordinate. Each macro-mechanical finite element coincides with the unique unit cell. Hence, this problem contains 435,074 independent degrees-of-freedom.

The multi-grid process was carried out on 4 different meshes: two-scale (macro-micro) mesh and three auxiliary macro-mechanical meshes. We used V-cycle with 1 pre- and 1 post- smoothing Gauss-Seidel iterations on the two auxiliary levels and 2 pre- and 2 post- smoothing Jacobi iterations on the finest level. As usual, on the coarsest level we used a direct solver. It was necessary to perform 15 multi-grid cycles to provide the convergence with $eps = 0.01$ in accordance with criteria (64). Only MLAT-Comp algorithm was tested, since the micro-grid contained over 100,000 nodes, and the direct solution on the micro-grid is not practical. This computational process takes about 8.2 hours on the SPARC station LX, which is 17.2 times faster than the use of a skyline direct solver and the storage savings are significant.

Appendix

Two dimensional idealization of $[90_p/0_q]_s$ laminated plate

Consider a $[90_p/0_q]_s$ laminated plate as shown in Fig. 9. The uniform axial tension is applied along the co-ordinate Z. In order to reduce the problem dimension to 2-D we assume that the shear stresses σ_{xz}, σ_{yz} and the shear strains ε_{xz}, ε_{yz} are negligible and it is necessary to idealize the microstructure in "90° layer" as a stack of orthotropic layers parallel to the interface.

For the purpose of calculating the equivalent mechanical properties of this layer, we consider the auxiliary problem given in Fig. 10. The elasticity moduli, the Poisson's ratios and the volume fractions are denoted by $(E_i, \nu_i$ and $k_i)$, $(i = 1, 2)$, respectively.

The homogenized elasticity moduli are found on the basis of the rule of mixtures:

$$E_x = E_y = k_1 E_1 + k_2 E_2 \qquad E_z = (k_1 E_1^{-1} + k_2 E_2^{-1})^{-1} \tag{65}$$

The Poisson's ratio in the plane XY is evaluated on the basis of the equilibrium condition along the co-ordinate Y under the uniform tension in X $(\varepsilon_x = 1)$:

$$k_1 E_1 (\nu_1 - \nu_{xy}) = k_2 E_2 (\nu_{xy} - \nu_2) \tag{66}$$

which yields

$$\nu_{xy} = \nu_{yx} = (k_1 E_1 \nu_1 + k_2 E_2 \nu_2)/E_x \tag{67}$$

Similarly, the equilibrium condition along the co-ordinate X under the uniform tension in Z $(\varepsilon_z = 1)$ yields

$$k_1 E_1 (e_1 - \nu_{xz}) = k_2 E_2 (\nu_{xz} - e_2)$$

$$e_1 = E_z \nu_1 / E_1 \qquad e_2 = E_z \nu_2 / E_2 \tag{68}$$

Exploiting the relation for orthotropic material, $E_z \nu_{zx} = E_x \nu_{xz}$, and using the symmetry condition in X and Y gives

$$\nu_{xz} = \nu_{yz} = E_z(k_1\nu_1 + k_2\nu_2)/E_x$$
$$\nu_{zx} = \nu_{zy} = k_1\nu_1 + k_2\nu_2$$

(69)

Equations (65), (67) and (69) represent the equivalent orthotropic material properties for the two-phase material described in Fig. 10.

In the second part of this appendix we will show that for the axial tension problem in the heterogeneous medium only a two-dimensional discretization is necessary.

Consider the two-scale asymptotic expansion of the strain field for the axial tension problem:

$$\varepsilon_{\alpha\beta} = (\delta_{\alpha\gamma}\delta_{\beta\delta} + h_{(\alpha,\beta)\gamma\delta})\varepsilon^0_{\gamma\delta} + h_{(\alpha,\beta)33}\varepsilon^0_{33} + O(\varepsilon)$$
$$= (\delta_{\alpha k}\delta_{\beta l} + h_{(\alpha,\beta)kl})\varepsilon^0_{kl} + O(\varepsilon)$$

(70)

and

$$\varepsilon_{33} = \varepsilon^0_{33} = const \qquad \varepsilon_{\alpha 3} = \varepsilon^0_{\alpha 3} = 0$$

(71)

where Greek subscripts range from one to two. The corresponding strain variation is given

$$\delta\varepsilon_{\alpha\beta} = (\delta_{\alpha\gamma}\delta_{\beta\delta} + h_{(\alpha,\beta)\gamma\delta})\delta\varepsilon^0_{\gamma\delta} + \delta h_{(\alpha,\beta)kl}\varepsilon^0_{kl}$$

(72)

while other components of the strain variation vanish.

For the axial tension problem in the uniform tension, $\varepsilon_{33} = \varepsilon^0_{33}$, and the weak form of equilibrium states that:

$$\int_\Omega \delta\varepsilon_{\alpha\beta}D_{\alpha\beta mn}\varepsilon_{mn}d\Omega = 0 \qquad \forall u \in C^o(\Omega)$$

(73)

Substituting (70) - (72) into (73) yields:

$$\int_\Omega ((\delta_{\alpha\gamma}\delta_{\beta\delta} + h_{(\alpha,\beta)\gamma\delta})\delta\varepsilon^0_{\gamma\delta} + \delta h_{(\alpha,\beta)kl}\varepsilon^0_{kl}) \times$$

(74)

$$(D_{\alpha\beta\xi\eta}(\delta_{\xi m}\delta_{\eta n} + h_{(\xi,\eta)mn}) + D_{\alpha\beta33}\delta_{3m}\delta_{3n})\varepsilon^0_{mn}d\Omega = 0$$

Applying the integration rule for highly oscillatory functions on θ [1] results in a

macro equilibrium equation:

$$\int_{\Omega_x} \delta\varepsilon^0_{\alpha\beta} \tilde{D}_{\alpha\beta\gamma\delta} \varepsilon^0_{\gamma\delta} d\Omega_x = -\int_{\Omega_x} \delta\varepsilon^0_{\alpha\beta} \tilde{D}_{\alpha\beta33} \varepsilon^0_{33} d\Omega_x \qquad \forall u \in C^o(\Omega) \tag{75}$$

where

$$\tilde{D}_{\alpha\beta\gamma\delta} = \frac{1}{\theta_Y}\int_\theta (\delta_{\alpha\nu}\delta_{\beta\mu} + h_{(\nu,\mu)\alpha\beta}) D_{\nu\mu\eta\xi} (\delta_{\gamma\eta}\delta_{\delta\xi} + h_{(\eta,\xi)\gamma\delta}) d\theta$$

$$\tilde{D}_{\alpha\beta33} = \frac{1}{\theta_Y}\int_\theta (\delta_{\alpha\nu}\delta_{\beta\mu} + h_{(\nu,\mu)\alpha\beta})(D_{\nu\mu\eta\xi} h_{(\eta,\xi)33} + D_{\nu\mu33}) d\theta \tag{76}$$

and micro (unit cell) equilibrium equations:

$$\int_\theta \delta h_{(\alpha,\beta)kl} D_{\alpha\beta\xi\eta} h_{(\xi,\eta)\nu\mu} d\theta = -\int_\theta \delta h_{(\alpha,\beta)kl} D_{\alpha\beta\nu\mu} d\theta \Rightarrow h_{\xi\nu\mu}$$

$$\int_\theta \delta h_{(\alpha,\beta)kl} D_{\alpha\beta\xi\eta} h_{(\xi,\eta)33} d\theta = -\int_\theta \delta h_{(\alpha,\beta)kl} D_{\alpha\beta33} d\theta \Rightarrow h_{\xi33} \tag{77}$$

For details on finite element discretization of macro and micro equations see [13].

Acknowledgments

References

1. A. Benssousan, J.L. Lions and G. Papanicoulau, Asymptotic analysis for periodic structures, North Holland, Amsterdam, 1978.

2. E. Sanchez-Palencia and A. Zaoui, Homogenization techniques for composites. Homogenization techniques for composite media, Springer-Verlag, Berlin, 1985.

3. N.S. Bakhvalov and G.P. Panasenko, Homogenization of periodic medium processes, Nauka, Moscow, 1984.

4. Z. Hashin, Theory of composite materials, in F.W.Wend, H. Liebowitz and N.Perrone, eds., Mechanics of composite materials, John Wiley, NY (1991).

5. E. Kröner, Bounds of effective elastic moduli of disordered materials, J. Mech. Phys. Solids, 25 (1977) 137.

6. J.Fish and V. Belsky, Multigrid method for periodic heterogeneous media. Part 1: Convergence studies for one-dimensional case, submitted to Computer Methods in Applied Mechanics and Engineering.

7. Achi Brandt, Multi-level adaptive solutions to boundary-value problems, Mathematics of Computations, 31 (1977) 333-390.

8. S.F. McCormick and J.W. Thomas, The fast adaptive composite grid (FAC) method for elliptic equations, Mathematics of Computation 46 (1986) 439-456.

9. Michael A. Heroux and J.W. Thomas, A comparison of FAC and PCG methods for solving composite grid problems, Communications in Applied Numerical Methods, 8 (1992) 573-583.

10. O.C. Zienkiewicz and J.Z. Zhu, Superconvergent derivative recovery techniques and a posteriori error estimation in the finite element method. Part 1: A general superconvergent recovery technique, CR/671/91 Institute of Numerical Methods in Engineering, University College of Swansea, U.K., 1991.

11. J. Fish and S. Markolefas, Adaptive s-method for linear elastostatics, 104 (1993) 363-396.

12. J.M. Guedes and N. Kikuchi, Preprocessing and postprocessing for materials based on the homogenization method with adaptive finite element methods, Comp. Meth. Appl. Mech. Engng. 83, 143-198.

13. J. Fish and A. Wagiman, Multiscale finite element method for a locally nonperiodic heterogeneous medium, Computational Mechanics: The International Journal 21 (1993) 1-17.
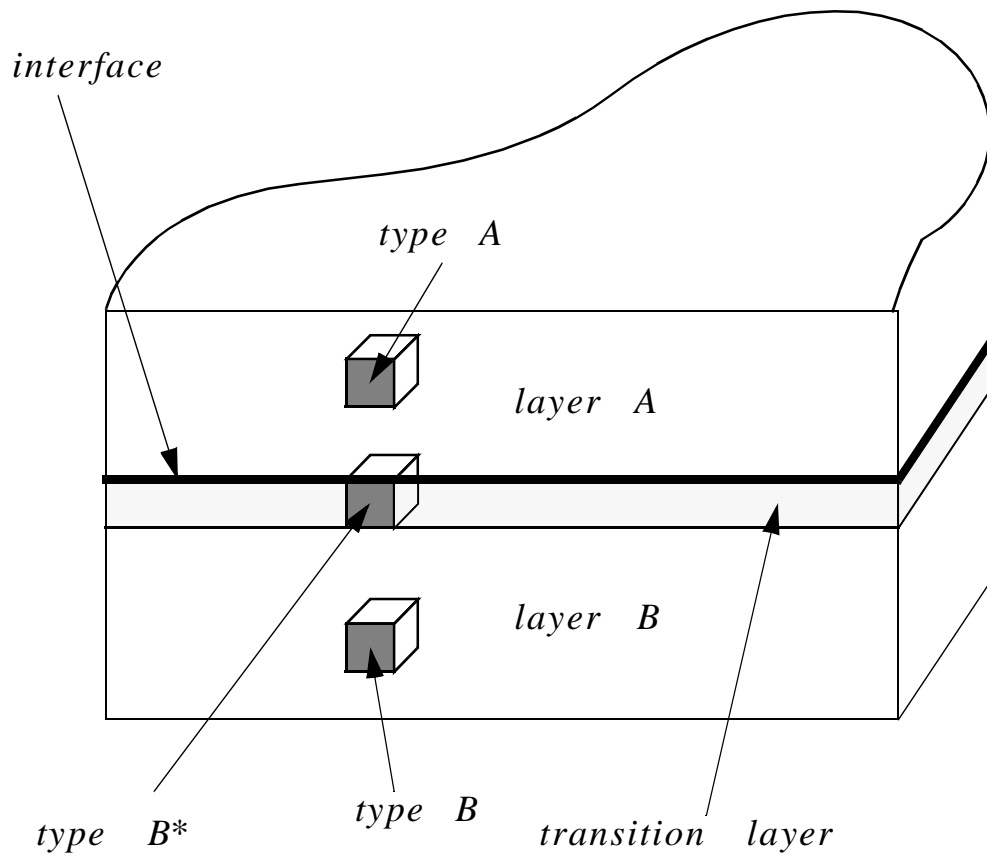
Fig. 2 *Partitioning of the auxiliary and micro grids*

$$\tilde{G}$$

$$\tilde{G}_G$$

$$\tilde{G}_I$$

$$G_I$$

$$\tilde{G}_L$$

$$G_L$$
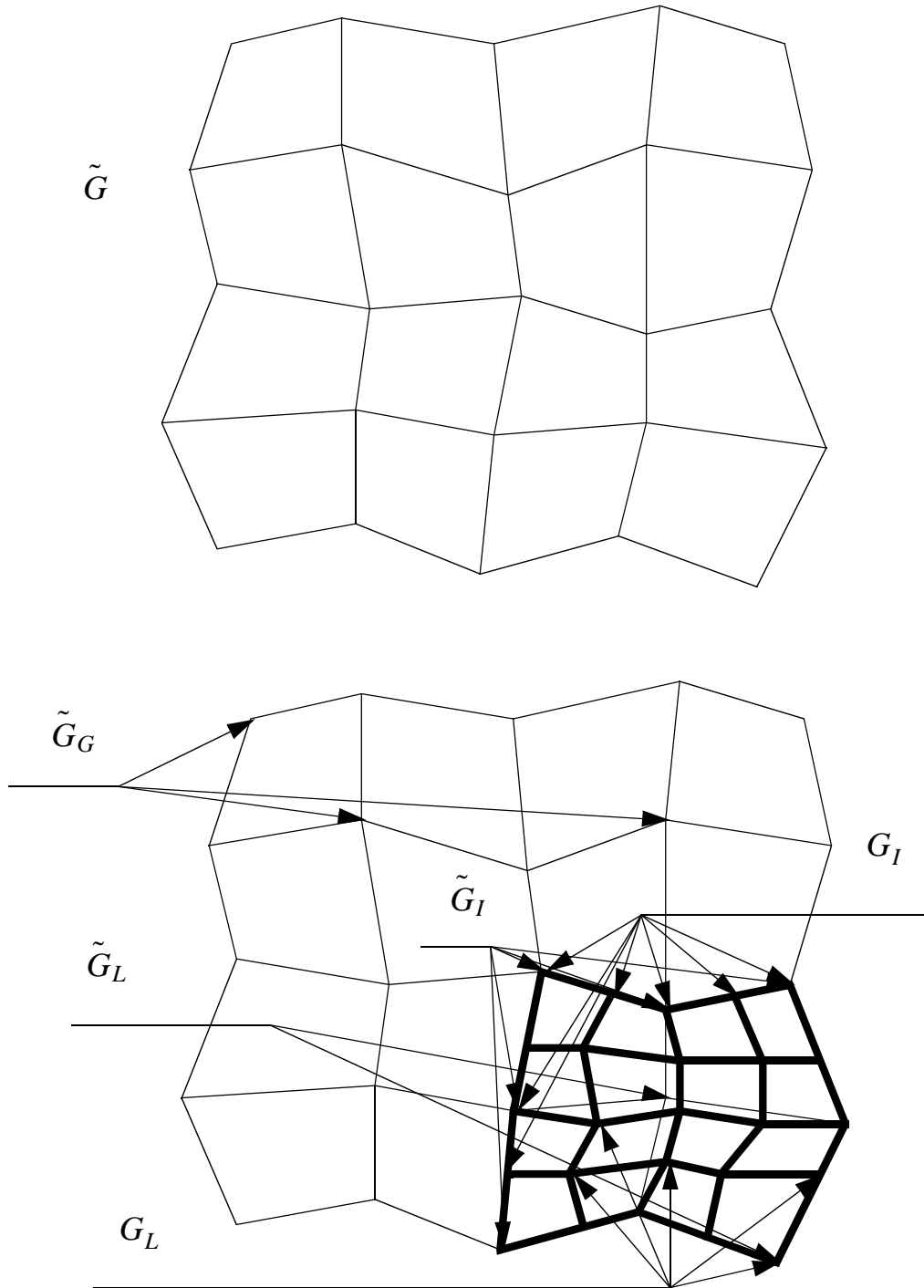
Fig. 3 *Plate with a centered crack: geometry, boundary conditions, material properties and loading*

crack tip

$E = 10$

$p = 1.0$

$E = 1.0$

x

$\nu = 0.3$

y

homogenization theory

micromechanical model
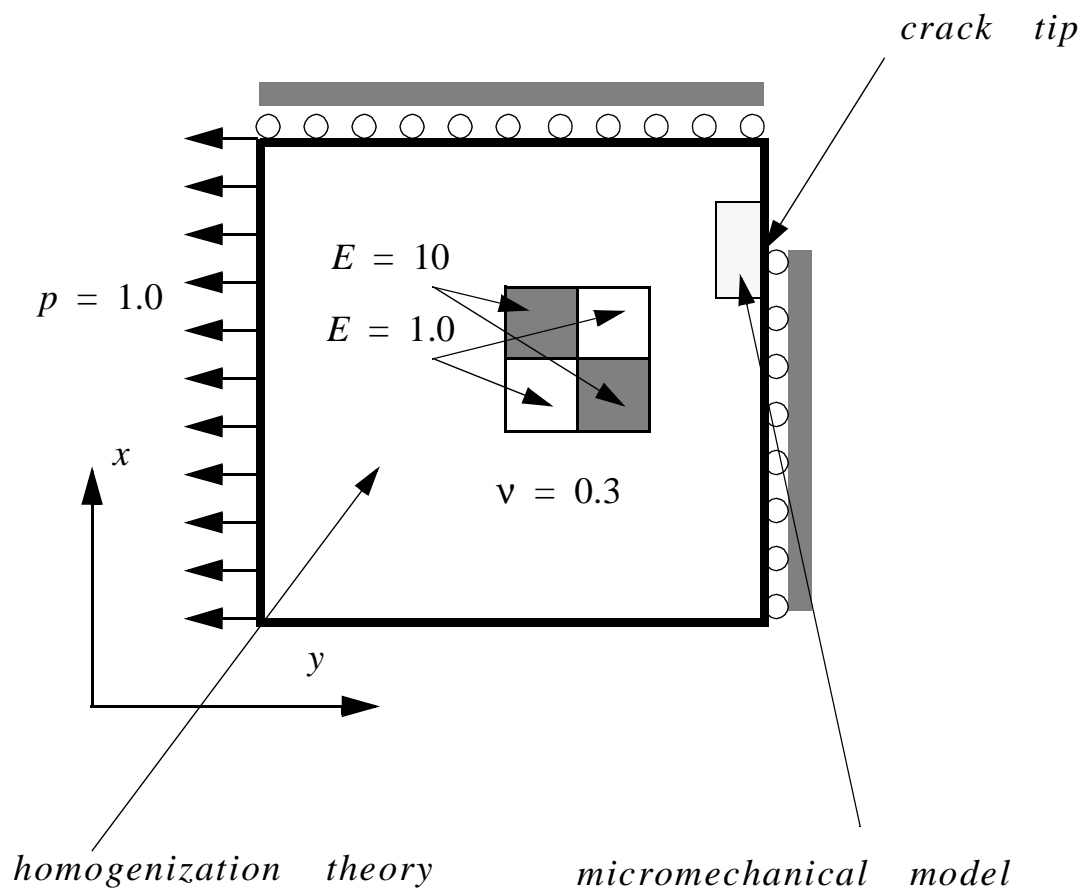
Fig. 4 *Microscale modelling of the plate with a centered crack and comparisons*

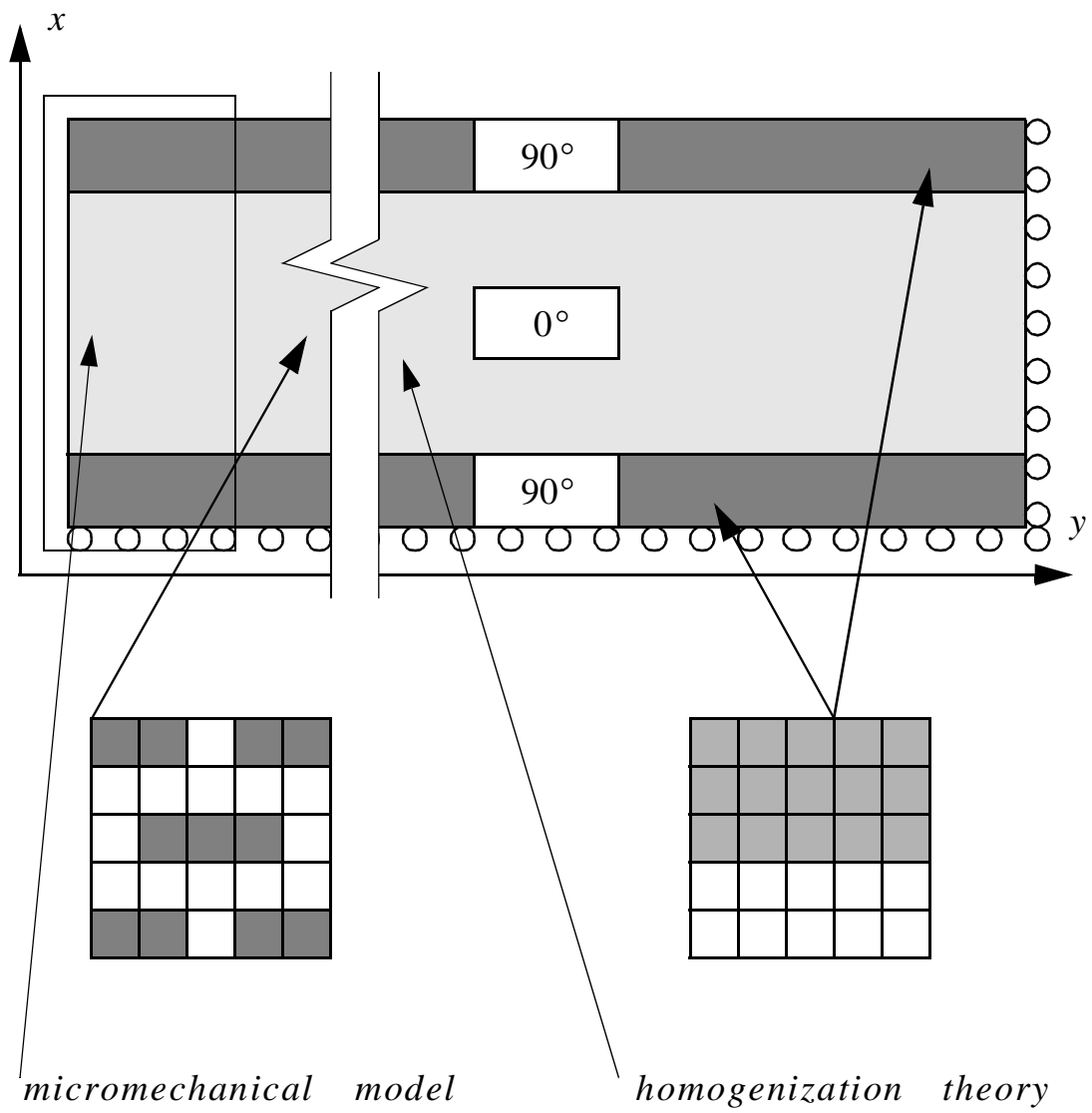*micromechanical   model*   *homogenization   theory*

Fig. 6 *Microscale modelling of the plate subjected to the axial tension and comparisons*

Fig. 7 *Plate subjected to the axial tension: the resulting peeling stresses*

Fig. 8 *Plate subjected to the axial tension: the resulting shear stresses*

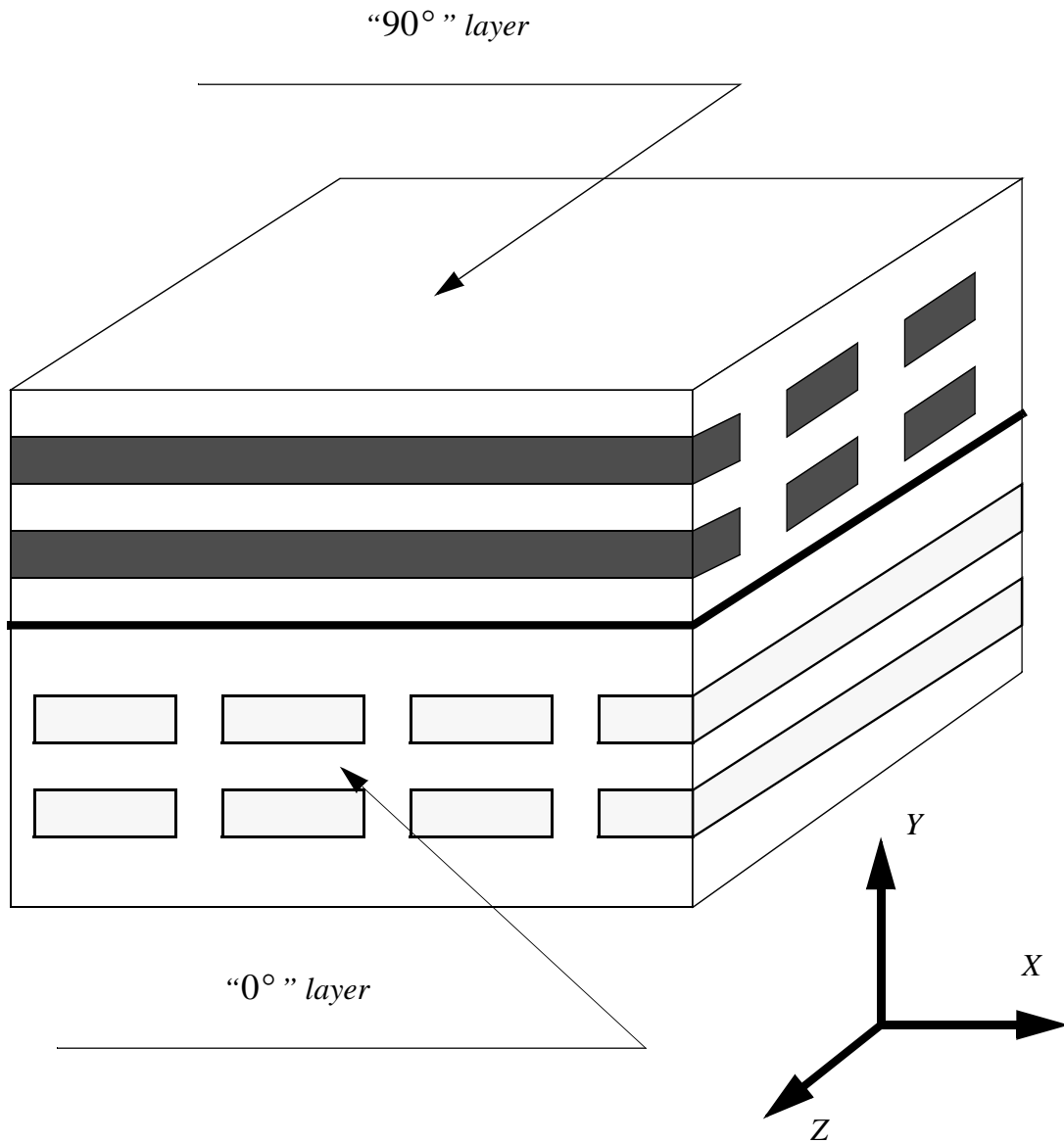Fig. 9 *Two dimensional idealization of the laminated plate*

Fig. 10 *The auxiliary problem for calculation of the equivalent mechanical properties*

E_1, ν_1, k_1

E_2, ν_2, k_2